Aftershock seismicity of the 2010 Maule Mw=8.8, Chile, earthquake: Correlation between co-seismic slip models and aftershock distribution?

A. Rietbrock, I. Ryder, G. Hayes, C. Haberland, D. Comte, S. Roecker, H
Lyon-Caen

Aftershock seismicity of the 2010 Maule Mw=8.8, Chile, earthquake: Correlation between co-seismic slip models and aftershock distribution?

A. Rietbrock,[1] I. Ryder,[1] G. Hayes,[2] C. Haberland,[3] D. Comte,[4] S. Roecker,[5] and H. Lyon-Caen[6,7]

[1] The 27 February 2010 Maule, Chile (Mw=8.8) earthquake is one of the best instrumentally observed subduction zone megathrust events. Here we present locations, magnitudes and cumulative equivalent moment of the first ∼2 months of aftershocks, recorded on a temporary network deployed within 2 weeks of the occurrence of the mainshock. Using automatically-determined onset times and a back projection approach for event association, we are able to detect over 30,000 events in the time period analyzed. To further increase the location accuracy, we systematically searched for potential S-wave arrivals and events were located in a regional 2D velocity model. Additionally, we calculated regional moment tensors to gain insight into the deformation history of the aftershock sequence. We find that the aftershock seismicity is concentrated between 40 and 140 km distance from the trench over a depth range of 10 to 35 km. Focal mechanisms indicate a predominance of thrust faulting, with occasional normal faulting events. Increased activity is seen in the outer-rise region of the Nazca plate, predominantly in the northern part of the rupture area. Further down-dip, a second band of clustered seismicity, showing mainly thrust motion, is located at depths of 40–45 km. By comparing recent published mainshock source inversions with our aftershock distribution, we discriminate slip models based on the assumption that aftershocks occur in areas of rapid transition between high and low slip, surrounding high-slip regions of the mainshock. **Citation:** Rietbrock, A., I. Ryder, G. Hayes, C. Haberland, D. Comte, S. Roecker, and H. Lyon-Caen (2012), Aftershock seismicity of the 2010 Maule Mw=8.8, Chile, earthquake: Correlation between co-seismic slip models and aftershock distribution?, *Geophys. Res. Lett.*, *39*, L08310, doi:10.1029/2012GL051308.

1. Introduction

[2] On 27 February 2010 a magnitude (M$_w$) 8.8 earthquake occurred along the South American subduction zone in the Central-South Chile region, rupturing approximately 400 km along the dipping mega-thrust interface (Figure 1). Prior to the 2010 large earthquake, the southern area of the rupture zone (south of 36°) had been recognized as one of the major seismic gaps along the Chilean subduction zone [e.g., *Campos et al.*, 2002]. To date, various co-seismic slip inversions based on seismological, geodetic (GPS), InSAR or tsunami data, or combinations of these datasets, have been published [e.g., *Delouis et al.*, 2010; *Lay et al.*, 2010; *Tong et al.*, 2010; *Lorito et al.*, 2011; *Vigny et al.*, 2011; *Pollitz et al.*, 2011]. While all inversions consistently show large slip in the north of the rupture area between 34°S and 35°S (slip of ∼20 m), models vary significantly in the south, ranging from featuring highly localized slip [e.g., *Delouis et al.*, 2010] to more uniformly-distributed slip [e.g., *Tong et al.*, 2010]. Additionally, slip models vary significantly with respect to where the largest slip occurs with depth (i.e., distance from the trench). For example, *Vigny et al.* [2011] estimate that a significant proportion of slip occurred between 0–50 km from the trench, while *Lorito et al.* [2011] found that the slip is concentrated deeper, along the subduction interface, at distances of 50–150 km from the trench (Figure 1). A precise understanding of the causes of these differences in slip distribution models is still lacking, and therefore a physical interpretation of slip with respect to fault zone mechanics is hindered. The distribution of aftershocks provides an independent tool to assess both the heterogeneous stress field caused by the rupture of the main shock, and/or the heterogeneous material properties along the interface. Additionally, they facilitate an accurate estimation of the detailed geometry of the megathrust fault, which is required as *a priori* information for all slip inversions.

[3] While it is widely accepted that the rupture process of the main shock and the associated static stress changes should govern the locations of aftershocks, direct qualitative or quantitative comparisons between co-seismic slip models and aftershock distributions are limited, especially for the case of large subduction zone earthquakes. Based on a small data ensemble of mostly subduction zone earthquakes, *Das and Henry* [2003] concluded that they could not find a general relation between high- and low-slip regions and high and low numbers of aftershocks. However, they found that generally fewer and smaller events occur in high slip regions and that clustered aftershock seismicity can be found in the areas of rapid transition between high and low slip on the main fault. *Woessner et al.* [2006] used statistical tests to quantify the correlation between slip and aftershock distribution along strike-slip faults and concluded that aftershocks are preferentially located in low-slip regions, supporting the

¹Department of Earth Sciences, University of Liverpool, Liverpool, UK.
²National Earthquake Information Center, U.S. Geological Survey, Denver, Colorado, USA.
³GeoForschungsZentrum Potsdam, Potsdam, Germany.
⁴AMTC, FCFM, University of Chile, Santiago, Chile.
⁵Rensselaer Polytechnic Institute, Troy, New York, USA.
⁶Laboratoire de Géologie, Ecole Normale Supérieure, CNRS, Paris, France.
⁷Laboratoire International Associé Montessus de Ballore, Paris, France.
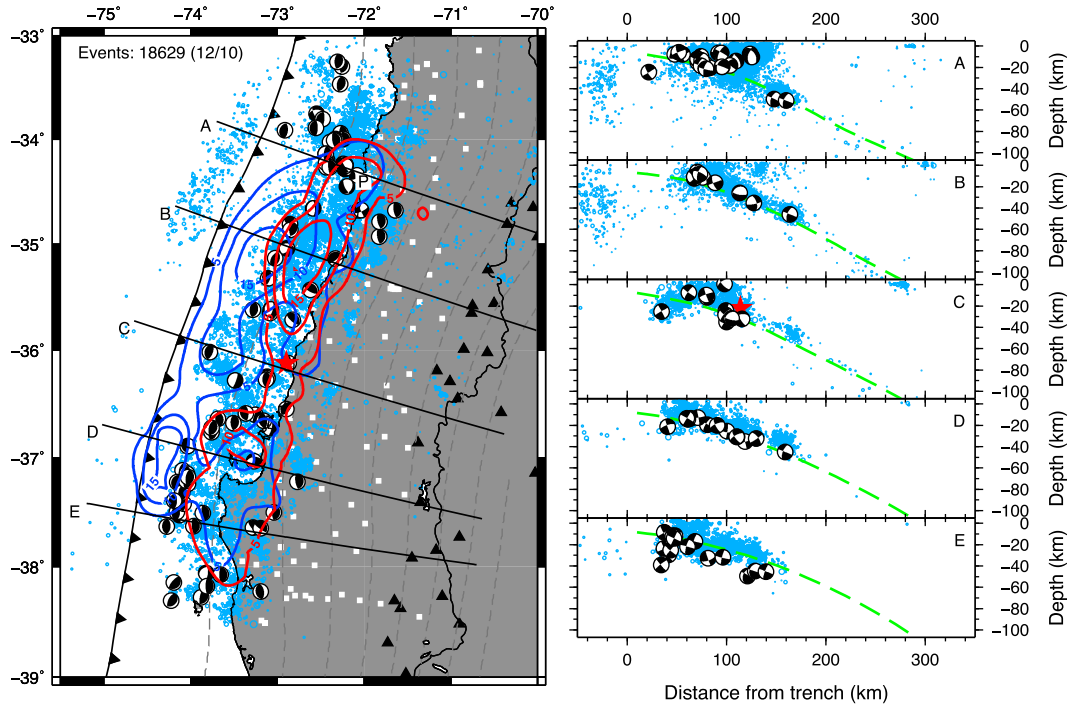
Figure 1. Seismic event locations (blue circles) based on automatic processing of the IMAD continuous waveform archive for the time period 15-3-2010 to 24-5-2010. Focal mechanisms inferred from regional moment tensor inversions are super-imposed at locations determined from IMAD. Active volcanoes are indicated as black triangles and white squares represent seismic stations. Corresponding cross-sections perpendicular to the trench (A to E) are shown on the right. Only events with at least 10 P and 10 S-wave observations are shown in the cross sections A to E. Distances are based on trench locations and the slab geometry was taken from SLAB 1.0 [*Hayes et al.*, 2012] and it is indicated in green. Focal mechanisms are projected into the plane and are viewed from the south. 5 m slip contours based on the slip model of *Vigny et al.* [2011] and *Lorito et al.* [2011] are shown in blue (model class C1) and red (model class C2), respectively. The red star indicates the hypocenter of the mainshock (NEIC). The label "P" indicates the area of Pichilemu.

results of *Das and Henry* [2003]. One of the most detailed studies of correlation between co- and post-seismic slip and aftershock locations was carried out for the 2005 Nias-Simeulue, Sumatra, (M_w = 8.7) earthquake [*Hsu et al.*, 2006]. This study found that aftershocks clustered along the boundary between the region of highest co-seismic slip and the up-dip post-seismic creeping zone. Recently, *Asano et al.* [2011] analyzed the spatial distribution and focal mechanisms of aftershocks of the March 2011 Tohoku-Oki, Japan, (M_w = 9.0) earthquake. They found that interplate aftershocks with thrust focal mechanisms did not occur within the area of large coseismic slip estimated from GPS data, but instead localized in the surrounding regions.

[4] Here we present locations, local magnitudes and cumulative equivalent moment estimates of the aftershock sequence that occurred within approximately the first two months of the mainshock (starting 15 March, two weeks after the main shock, until 24 May 2010). All events were recorded on the International Maule Aftershock Dataset (IMAD) network. We also present focal mechanisms for the largest events during this time period, based on regional moment tensor inversions. We then compare the obtained aftershock distribution and cumulative moment estimates with currently published co-seismic slip models. Based on the assumption that aftershocks occur in areas of rapid transition between high and low slip surrounding high-slip

regions, we attempt to resolve discrepancies between contrasting slip distributions.

2. Data and Processing

[5] Immediately following the 27 February 2010 Maule earthquake (M_w = 8.8), a multinational effort of Chilean Universities; Incorporated Research Institutions for Seismology (IRIS), US; the CNRS-INSU, France; the Geo Forschungs Zentrum Potsdam (GFZ), Germany; and the University of Liverpool, UK, deployed in close collaboration a dense seismic network to record aftershock activity. A total of more than 160 seismic stations - mainly broadband sensors - were deployed (Figure 1), spanning the entire onland extent of the co-seismic rupture. The datasets from all agencies were compiled into the International Maule Aftershock Dataset (IMAD). For obtaining locations of these largely offshore aftershocks we used a staggered approach to determine and associate P and S arrival times. We automatically detected seismic arrival times based on calculations of the short-term versus long-term average ratio (STA/LTA trigger) on vertical component seismograms. In total more than 2,300,000 arrival times of potential P-wave and S-wave onsets were detected. A back projection technique in a 1D velocity model was used for the event association and preliminary hypocenters were determined. Based on the initial locations a more sensitive STA/LTA trigger was deployed to increase

the number of onset times and especially the number of S-wave onsets. Events were relocated in the same 1D model and we selected events with an azimuthal gap of less than 270 degrees and with at least 12 P wave onset times for further processing. In a final location step all events were relocated in a 2D velocity model. The 2D velocity model is based predominantly on the tomographic model for P-wave velocity and Vp/Vs ratio of *Haberland et al.* [2009] and is extended westward from the trench using the wide-angle refraction profile of *Contreras-Reyes et al.* [2008]. Since most of the aftershock activity is located offshore, tests also showed that S-wave arrivals are essential for estimating their locations, since it is not possible to apply a stringent azimuthal gap criterion of less than 180°. Using only P-wave arrivals led to a blurred image of the seismicity distribution and systematic errors in the depth of some features, as can be seen in the auxiliary material.[1] In total we present 18,629 aftershocks with their event locations constrained by approximately 40 P and 20 S wave onset times. Local magnitudes based on automatically determined peak-to-peak amplitudes and associated frequency were calculated using the relationship of *Bakun and Joyner* [1984].

[6]   To supplement our observations, we calculated regional moment tensor (RMT) inversions based on *Herrmann et al.* [2011] of all Preliminary Determination of Epicenters (PDE) catalogue earthquakes of M ≥ 4.5. Using the calculated M_w values we also derived a linear relationship between local and moment magnitude $M_w = 1.17 * Ml - 1.43$, and this relationship was used to calculate cumulative aftershock moment (and the associated slip on the plate interface) during the observation period. The detailed processing scheme is described in the supplementary information.

3.   Results and Discussion

[7]   The located aftershock seismicity between 15 March and 24 May 2010 is shown in Figure 1, where the focal mechanisms obtained from RMT inversions are superimposed. Seismicity along cross-sections A-E reveals aftershocks that are mostly concentrated between 40 and 140 km distance from the trench in a depth range of 10 to 35 km. Focal mechanisms indicate a predominance of thrust faulting, with occasional normal faulting events; most of the latter are related to the Pichilemu aftershocks that were triggered on March 11, 2010 by the mainshock [*Farías et al.*, 2011; *Ryder et al.*, 2012]. There is also an increase of seismic activity observed in the outer-rise region of the Nazca plate, predominantly in the northern part of the rupture area. Further down-dip, a second band of seismicity (clearly separated from the main activity on cross-sections A-D) is located at depths of 40–45 km. Seismicity at this depth range is not continuous along strike but concentrated in spatially separated clusters. Focal mechanisms for three of the cluster events indicate thrust motions, suggesting that they occur along the plate interface (interplate events). Clustered seismicity is also observed beneath the active volcanic front, with event magnitudes of less than Ml = 3. Crustal seismicity in the overriding South American plate is mostly concentrated in the area of Pichilemu (labelled "P" in Figure 1) at the northern end of rupture area (profiles A & B

in Figure 1). While in the north and south of the rupture area (profiles A & E) the seismicity depth distribution follows the global slab model SLAB1.0 [*Hayes et al.*, 2012], the seismicity in the central part is predominantly above the modelled plate boundary, suggesting local slab interface topography on the order of a few kilometres.

[8]   As stated previously, many slip models have been published already; most are summarized by *Vigny et al.* [2011]. All of them show the largest slip in the north of the rupture area but vary considerably in their representation of slip to the south, near the Arauco Peninsula. Despite these variations they can be classified into two model classes. Class one (C1) are slip models that locate the largest slip close to the trench (0–50 km from the trench [e.g., *Vigny et al.*, 2011; *Lay et al.*, 2010]); class two models (C2) show the largest slip located further away from the trench (50–100 km [e.g., *Lorito et al.*, 2011; *Delouis et al.*, 2010]) at greater depth. These two classes of slip model are compared with the number of aftershocks and their associated post-seismic cumulative moment estimates in the central part of the rupture (Figure 2), projected along profiles B, C, D, and an average over the whole rupture length (Total). The cumulative moment of aftershocks was calculated using our M_w estimates and an empirical scaling relationship between M_w and source area to account for extended sources [*Mai and Beroza*, 2000] was derived. To calculate the average cumulative moment along each cross-section, we projected seismicity within ±15 km of each profile and averaged the results with a 10 km wide sliding window in the down-dip direction (black curve in Figure 2). The cumulative moment estimates of the aftershock sequence are dominated by the largest aftershocks for which we calculated RMT solutions and are a direct measure of the seismic slip associated with this seismicity.

[9]   For C1 models, a significant amount of co-seismic slip occurs in an area with very little aftershock activity (0–50 km from the trench), clearly observed in all cross sections (blue curves in Figure 2). This region, corresponding to the outer part of the marine forearc, has been described previously as an 'aseismic' band, for which the eastern border coincides with temperatures of 100–150°C at the plate interface [*Haberland et al.*, 2009]. The lack of seismicity in this band can be explained by the velocity strengthening and therefore stable sliding frictional properties of clay rich sediments contained in the outer marine forearc [e.g., *Saffer and Marone*, 2003]. Recent observations for the Tohoku-Oki earthquake [*Simons et al.*, 2011] and the 2010 Mentawai earthquake [*Collings et al.*, 2012; *Newman et al.*, 2011] demonstrate that the outer part of the marine forearc can produce significant slip during large earthquakes, but does not show significant minor seismicity during the interseismic cycle. It should be noted that for cross sections C and D, minor seismicity is observed in the outer marine forearc, but these events do not contribute significantly to the overall cumulative post-seismic moment of aftershocks (black curve in Figure 2, total). For model class C2, the area of modelled large co-seismic slip primarily overlaps with the region of largest cumulative moment of aftershocks (red and black curve in Figure 2, respectively). Relatively small co-seismic slip values (<4 m) are observed close to the trench, while the maximum average slip located at about 100 km distance from the trench correlates closely with the region of maximum

---

[1]Auxiliary materials are available in the HTML. doi:10.1029/2012GL051308.
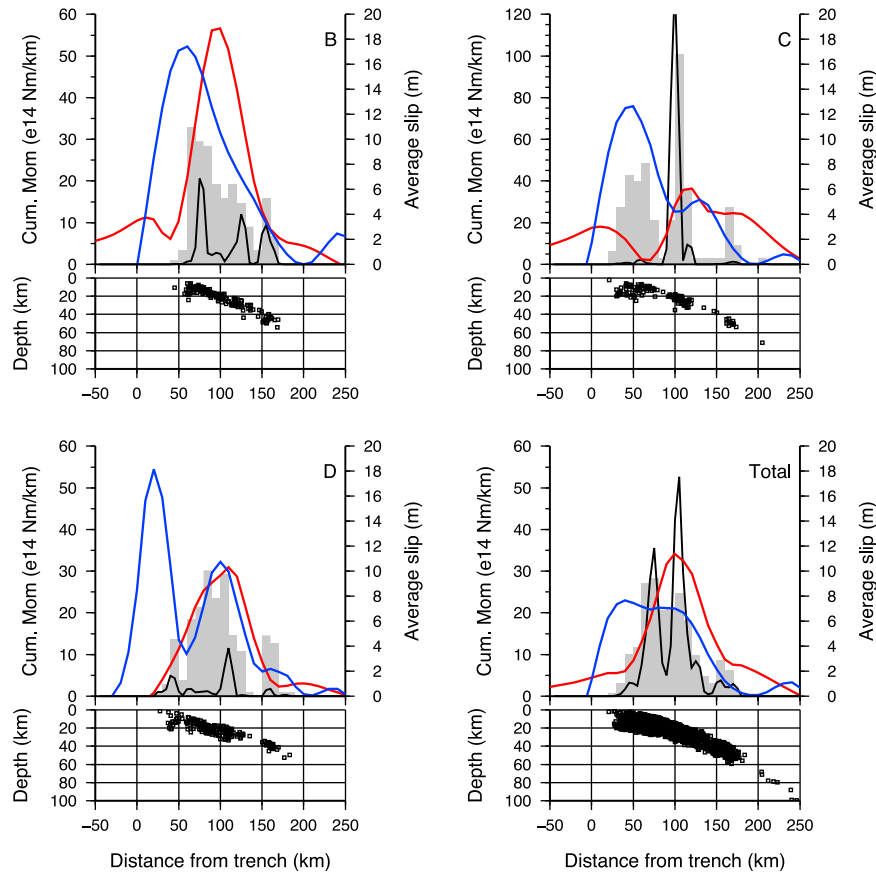
Figure 2. Comparison between the number of events plotted as percentage values (gray histogram) and average co-seismic slip taken from various slip models as a function of distance from the deformation front. The slip models of *Vigny et al.* [2011] and *Lorito et al.* [2011] are shown in blue and red, respectively. The black lines represent average cumulative moment release based on our moment estimates. Only events that are located in a depth corridor of +/−10 km from the predicted slab interface (SLAB 1.0) are taken into account for the average moment release and event histogram. Cross sections show the distribution of these events along each of the profiles (B, C, D, and Total).

cumulative moment of aftershocks when averaged along the strike of the rupture plane (Figure 2, Total).

[10] For large subduction zone interplate earthquakes in general, it is widely accepted that the main shock releases a large fraction of strain accumulated during the interseismic cycle. Aftershock seismicity (especially the largest events) should therefore be predominantly located in areas of transition between high and low slip, surrounding high-slip regions. Using such a definition and the location of aftershocks and associated cumulative moment release, we can judge the quality of the two classes of slip model C1 and C2 for the Maule mainshock. For model class C1, co-seismic slip is generally located up-dip of the aftershock distribution (Figure 2), and a significant fraction of slip is located close to the trench, implying that aftershocks are located in the down-dip transition from high to low slip, nearer the down dip end of the seismogenic zone. In contrast, comparison of the aftershock distribution with model class C2 (based on averaging the co-seismic slip and the cumulative aftershock moment along strike; Figure 2, Total), would imply that most of the aftershocks and their cumulative moment occurs in the same depth interval responsible for the largest slip. Given the amount of slip during the mainshock, and the time since the last earthquake on this section of the plate boundary (1835), this latter explanation seems less likely.

However, individual cross sections (e.g., Figure 2, profiles B and D) suggest that the largest cumulative aftershock moment is located on the up- and down-dip edges of local patches of highest slip for model class C2. Therefore, if the co-seismic slip was indeed localized in discrete patches along strike – a feature that may not be definitely resolvable in some slip inversions, including those used for model class C2, due to the resolution of inverted datasets and the imposed model regularization – a refined model class C2 may also explain the aftershock distribution.

[11] For model class C1 we also note that an overlap exists between aftershock activity and areas of larger slip in the down-dip region of the rupture plane. However, this area coincides with large variations in slip (e.g., cross section B) and therefore increased aftershock activity in this depth range might be expected. Based on the available slip models and aftershock distribution our analysis supports the findings of *Das and Henry* [2003] that aftershocks are located in the region of rapid transition from high to low slip. Whether or not aftershocks of the Maule earthquake are located preferentially in areas of low slip, as was suggested by *Woessner et al.* [2006] for strike-slip fault systems, cannot be sufficiently resolved with the currently available slip models.

[12] The location of slip for the 2010 Maule earthquake with respect to the trench position is also a very important

issue for assessing the future tsunamigenic potential in this area. If the 2010 Maule earthquake had significant slip near the trench (C1), the likelihood of a major tsunamigenic earthquake in the near future might be lower. On the other hand if the slip was mainly concentrated further down-dip (C2) the opposite might be true and there may now be an increased tsunami hazard for this region, depending on the interface properties at shallow depth. A more detailed analysis of the co-seismic slip model using all available tsunami, geodetic, and seismic recordings together with the after-shock distribution is urgently needed to resolve this issue.

[14] The Editor thanks two anonymous reviewers for their assistance in evaluating this paper.

References

Asano, Y., et al. (2011), Spatial distribution and focal mechanisms of aftershocks of the 2011 off the Pacific coast of Tohoku earthquake, *Earth Planets Space*, *63*, 669–673, doi:10.5047/eps.2011.06.016.

Bakun, W. H., and W. B. Joyner (1984), The Ml scale in central California, *Bull. Seismol. Soc. Am.*, *74*, 1827–1843.

Campos, J., et al. (2002), A seismological study of the 1835 seismic gap in south-central Chile, *Phys. Earth Planet. Inter.*, *132*, 177–195, doi:10.1016/S0031-9201(02)00051-1.

Collings, R., D. Lange, A. Rietbrock, F. Tilmann, D. Natawidjaja, B. Suwargadi, M. Miller, and J. Saul (2012), Structure and seismogenic properties of the Mentawai segment of the Sumatra subduction zone revealed by local earthquake traveltime tomography, *J. Geophys. Res.*, *117*, B01312, doi:10.1029/2011JB008469.

Contreras-Reyes, E., I. Grevemeyer, E. F. Flueh, M. Scherwath, and J. Bialas (2008), Effect of trench-outer rise bending-related faulting on seismic Poisson's ratio and mantle anisotropy: A case study offshore of southern central Chile, *Geophys. J. Int.*, *173*, 142–156, doi:10.1111/j.1365-246X.2008.03716.x.

Das, S., and C. Henry (2003), Spatial relation between main earthquake slip and its aftershock distribution, *Rev. Geophys.*, *41*(3), 1013, doi:10.1029/2002RG000119.

Delouis, B., J.-M. Nocquet, and M. Vallée (2010), Slip distribution of the February 27, 2010 Mw = 8.8 Maule earthquake, central Chile, from static and high-rate GPS, InSAR, and broadband teleseismic data, *Geophys. Res. Lett.*, *37*, L17305, doi:10.1029/2010GL043899.

Farías, M., D. Comte, S. Roecker, D. Carrizo, and M. Pardo (2011), Crustal extensional faulting triggered by the 2010 Chilean earthquake: The Pichilemu Seismic Sequence, *Tectonics*, *30*, TC6010, doi:10.1029/2011TC002888.

Haberland, C., A. Rietbrock, D. Lange, K. Bataille, and T. Dahm (2009), Structure of the seismogenic zone of the southcentral Chilean margin revealed by local earthquake traveltime tomography, *J. Geophys. Res.*, *114*, B01317, doi:10.1029/2008JB005802.

Hayes, G. P., D. J. Wald, and R. L. Johnson (2012), Slab1.0: A new three-dimensional model of global subduction interface geometry, *J. Geophys. Res.*, *117*, B01302, doi:10.1029/2011JB008524.

Herrmann, R. B., L. Malagnini, and I. Munafo (2011), Regional moment tensors of the 2009 L'Aquila earthquake sequence, *Bull. Seismol. Soc. Am.*, *101*(3), 975–993, doi:10.1785/0120100184.

Hsu, Y. J., et al. (2006), Frictional afterslip following the 2005 Nias-Simeulue earthquake, *Sumatra, Science*, *312*, 1921, doi:10.1126/science.1126960.

Lay, T., C. J. Ammon, H. Kanamori, K. D. Koper, O. Sufri, and A. R. Hutko (2010), Teleseismic inversion for rupture process of the 27 February 2010 Chile (Mw 8.8) earthquake, *Geophys. Res. Lett.*, *37*, L13301, doi:10.1029/2010GL043379.

Lorito, S., F. Romano, S. Atzori, X. Tong, A. Avallone, J. McCloskey, M. Cocco, E. Boschi, and A. Piatanesi (2011), Limited overlap between the seismic gap and coseismic slip of the great 2010 Chile earthquake, *Nat. Geosci.*, *4*, 173–177, doi:10.1038/ngeo1073.

Mai, P. M., and G. C. Beroza (2000), Source scaling properties from finite-fault-rupture models, *Bull. Seismol. Soc. Am.*, *90*(3), 604–615, doi:10.1785/0119990126.

Newman, A. V., G. Hayes, Y. Wei, and J. Convers (2011), The 25 October 2010 Mentawai tsunami earthquake, from real-time discriminants, finite-fault rupture, and tsunami excitation, *Geophys. Res. Lett.*, *38*, L05302, doi:10.1029/2010GL046498.

Pollitz, F. F., et al. (2011), Coseismic slip distribution of the February 27, 2010 Mw 8.8 Maule, Chile earthquake, *Geophys. Res. Lett.*, *38*, L09309, doi:10.1029/2011GL047065.

Ryder, I., R. Rietbrock, K. Kelson, R. Burgmann, M. Floyd, A. Socquet, C. Vigny, and D. Carrizo (2012), Large extensional aftershocks in the continental forearc triggered by the 2010 Maule earthquake, Chile, *Geophys. J. Int.*, *188*(3), 879–890, doi:10.1111/j.1365-246X.2011.05321.x.

Saffer, D. M., and C. Marone (2003), Comparison of Smectite- and Illite-rich gouge frictional properties: Application to the updip limit of the seismogenic zone along subduction megathrusts, *Earth Planet. Sci. Lett.*, *215*(1–2), 219–235, doi:10.1016/S0012-821X(03)00424-2.

Simons, M., et al. (2011), The 2011 magnitude 9.0 Tohoku-Oki earthquake: Mosaicking the megathrust from seconds to centuries, *Science*, *332*, 1421, doi:10.1126/science.1206731.

Tong, X., et al. (2010), The 2010 Maule, Chile earthquake: Downdip rupture limit revealed by space geodesy, *Geophys. Res. Lett.*, *37*, L24311, doi:10.1029/2010GL045805.

Vigny, C., et al. (2011), The 2010 Mw 8.8 Maule megathrust earthquake of central Chile, monitored by GPS, *Science*, *332*, 1417, doi:10.1126/science.1204132.

Woessner, J., D. Schorlemmer, S. Wiemer, and P. M. Mai (2006), Correction to "Spatial correlation of aftershock locations and on-fault main shock properties," *J. Geophys. Res.*, *111*, B09399, doi:10.1029/2006JB004676.

D. Comte, AMTC, FCFM, University of Chile, Blanco Encalada 2002, Santiago Casilla 2777, Correo 21, Santiago, Chile.

C. Haberland, GeoForschungsZentrum Potsdam, Telegrafenberg, D-14473 Potsdam, Germany.

G. Hayes, National Earthquake Information Center, U. S. Geological Survey, PO Box 25046, MS 966, Denver, CO 80225, USA.

H. Lyon-Caen, Laboratoire de Géologie, Ecole Normale Supérieure, CNRS, 24 rue Lhomond, F-75231 Paris CEDEX, France.

A. Rietbrock and I. Ryder, Department of Earth Sciences, University of Liverpool, 4 Brownlow St., Liverpool L69 3GP, UK. (a.rietbrock@liverpool.ac.uk)

S. Roecker, Rensselaer Polytechnic Institute, 110 8th St., Troy, NY 12180, USA.